

# Effect of the Structural Properties on the Electrical Resistivity of the Al/Ag Thin Films during the Solid-State Reaction

R. R. Altunin<sup>a,\*</sup>, E. T. Moiseenko<sup>a</sup>, and S. M. Zharkov<sup>a,b</sup>

<sup>a</sup> Siberian Federal University, Krasnoyarsk, 660041 Russia

<sup>b</sup> Kirensky Institute of Physics, Krasnoyarsk Scientific Center, Siberian Branch, Russian Academy of Sciences, Krasnoyarsk, 660036 Russia

\*e-mail: [raltunin@gmail.com](mailto:raltunin@gmail.com)

Received December 16, 2019; revised December 16, 2019; accepted December 17, 2019

**Abstract**—Based on the results of in situ electron diffraction study of the solid-state reaction and electrical resistivity measurements on the Al/Ag thin films with an atomic ratio of Al : Ag = 1 : 3, the temperature of the reaction onset has been established and a model of the structural phase transitions has been proposed. The solid-state reaction begins at 70°C with the formation of the Al–Ag solid solution at the interface between the aluminum and silver nanolayers. It has been found that, in the course of the reaction, the intermetallic compounds  $\gamma$ -Ag<sub>2</sub>Al  $\rightarrow$   $\mu$ -Ag<sub>3</sub>Al are successively formed. It is shown that the possibility of the formation of the  $\mu$ -Ag<sub>3</sub>Al phase during the solid-state reaction in the Al/Ag thin films depends on the aluminum-to-silver ratio, while the formation of the  $\mu$ -Ag<sub>3</sub>Al phase begins only after all fcc aluminum has reacted.

**Keywords:** thin films, phase formation, Al/Ag, solid-state reaction, electron diffraction, resistivity

**DOI:** 10.1134/S1063783420040034

## 1. INTRODUCTION

The aluminum-containing compounds are of great interest for the microelectronic industry. They are used as electric compounds, diffusion barriers, and materials for enhancing the stability against electromigration [1–5]. The Al–Ag intermetallics are promising for application in microelectronic devices [6] and light emitting diodes [7–10]. Owing to their high oxidation resistance [11, 12] and reflectivity [13], the Al–Ag intermetallics can be used as reflective coatings of solar cells [14–16]. A fraction of microelectronic devices containing the Al–Ag compounds in the form of thin (up to 100 nm) films increases. On the other hand, the stability of the physicochemical properties of thin-film systems ensures the reliability of microelectronic devices containing these compounds. The solid-state reactions at the interface of thin-film systems can occur at relatively low temperatures (0.1–0.5 of melting points  $T_{\text{melt}}$  of constituents) [17], which leads to the formation of new compounds with different physicochemical properties. For example, even at room temperature at the interface of the Al/Au thin films the Al<sub>2</sub>Au intermetallic phase forms [18, 19], the electrical resistance of which is much higher than that of pure aluminum and gold [20]; this causes a failure of microwave transistors [21] containing these materials.

According to the phase diagram of the Al–Ag system, the intermetallic compounds that can form in it are the  $\gamma$ -Ag<sub>2</sub>Al phase (sp. gr.  $P6_3/mmc$ ,  $a = 2.885 \text{ \AA}$ , and  $c = 4.624 \text{ \AA}$ ), the high-temperature  $\beta$ -Ag<sub>3</sub>Al phase (sp. gr.  $Im\bar{3}m$ ,  $a = 3.243 \text{ \AA}$ ), and the low-temperature  $\mu$ -Ag<sub>3</sub>Al phase (sp. gr.  $P4132$ ,  $a = 6.946 \text{ \AA}$ ). The  $\mu$ -Ag<sub>3</sub>Al phase is of greater interest, since it has higher reflectivity, significantly higher hardness, and lower fracture toughness than the  $\gamma$ -Ag<sub>2</sub>Al phase [2].

Analysis of the experimental data shows that, during the solid-state reaction, two intermetallic compounds usually formed in the thick ( $\sim 1 \text{ \mu m}$ ) films are  $\gamma$ -Ag<sub>2</sub>Al and  $\mu$ -Ag<sub>3</sub>Al [15, 16, 22]. However, in the overwhelming majority of studies [23–25] devoted to the solid-phase interactions in the Ag/Al thin films with a thickness of up to 100 nm, the formation of the  $\mu$ -Ag<sub>3</sub>Al phase was not observed. In [22], the solid-state reactions in the Ag/Al films were studied by the Rutherford backscattering and X-ray diffraction techniques. The formation of the  $\gamma$ -Ag<sub>2</sub>Al intermetallic at a temperature of 150°C was reported and the presence of a small (1–2%) amount of the  $\mu$ -Ag<sub>3</sub>Al phase was suggested. One is interested in the conditions of formation of this phase in the thin-film systems and its electrical properties.

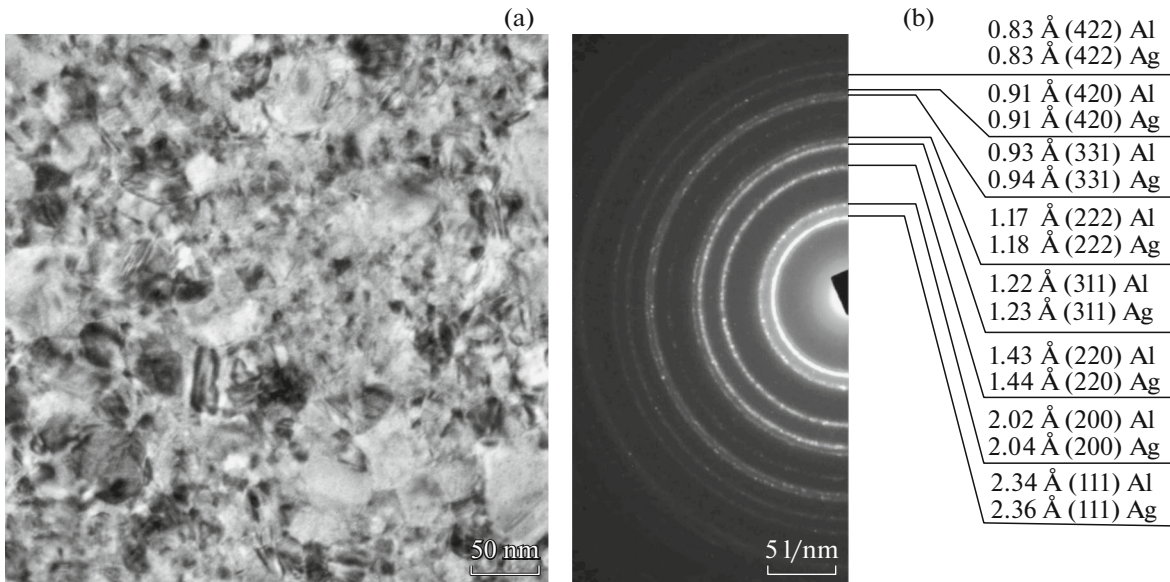


Fig. 1. (a) Electron microscopy image and (b) electron diffraction pattern of the initial Al/Ag film.

## 2. EXPERIMENTAL

The investigated Al/Ag thin films were obtained by magnetron sputtering on an EPOS-PVD-D-CONFOCAL high-vacuum facility. The basic residual pressure was  $1 \times 10^{-4}$  Pa and the argon pressure during sputtering was 0.26 Pa. The film thickness was controlled using a Bal-Tec QSG-100 quartz crystal thickness monitor, which allows one to control the integral film thickness accurate to 0.01 nm. The material deposition rate was 0.05–0.1 nm/s. The high-purity initial materials (Girmet Ltd.) Ag (99.99%) and Al (99.999%) were used. The substrates used for the film deposition were glass and electron microscopy grids coated with a thin ( $\approx 20$  nm) amorphous carbon layer. The 60-nm silver and 20-nm aluminum layers were deposited sequentially without interrupting the vacuum. To avoid a reaction between silver and aluminum, the silver layer was deposited first. The Al : Ag atomic ratio was 1 : 3.

The microstructure and elemental composition of the films were studied using a JEOL JEM-2100 transmission electron microscope at an accelerating voltage of 200 kV equipped with an Oxford Inca x-sight energy dispersive spectrometer. The phase composition of the samples was determined by analyzing the electron diffraction patterns obtained by the microdiffraction method. Heating was performed directly in the column of a JEM-2100 transmission electron microscope (a residual pressure of  $1 \times 10^{-6}$  Pa) using a special Gatan Model 652 Double Tilt Heating sample holder designed for controlled heating of samples from room temperature to 1000°C. This method was successfully used to study the solid-state reactions in the Fe/Pd

[26–28], Fe/Si [29], Al/Fe [30], Al/Cu [31], Fe–ZrO<sub>2</sub> [32], and Co–ZrO<sub>2</sub> thin films [33].

The simultaneous measurements of the electrical resistivity and temperature of the samples were performed using a Keithley 2450 sourcemeter and a Keithley DMM6500 digital multimeter. The electrical resistance was measured by the four-probe method.

## 3. EXPERIMENTAL RESULTS AND DISCUSSION

The electron microscopy investigations of the initial Al/Ag thin films revealed an aluminum crystallite size of  $10 \pm 3$  nm and a silver crystallite size of  $30 \pm 10$  nm (Fig. 1a). Since the lattice parameters of aluminum (sp. gr.  $Fm\bar{3}m$ , the lattice parameter is  $a = 4.049$  Å) and silver (sp. gr.  $Fm\bar{3}m$ , the lattice parameter is  $a = 4.086$  Å) differ by only 0.9%, it is almost impossible to distinguish the aluminum and silver diffraction reflections by the electron diffraction method. In the electron diffraction pattern (Fig. 1b), the polycrystalline reflections from the Al and Ag phases overlap, which leads to a slight broadening of the observed diffraction reflections.

To obtain information about the structural variations in the Al/Ag films during the solid-state reaction, we examined the phase formation upon heating the samples from room temperature to 300°C. The heating rate was 4°C/min. During heating, electron diffraction patterns were recorded at a rate of 4 fpm; i.e., one frame corresponded to the change in the sample temperature by 1°C. This allowed us to establish the temperature of the onset of the crystalline phase

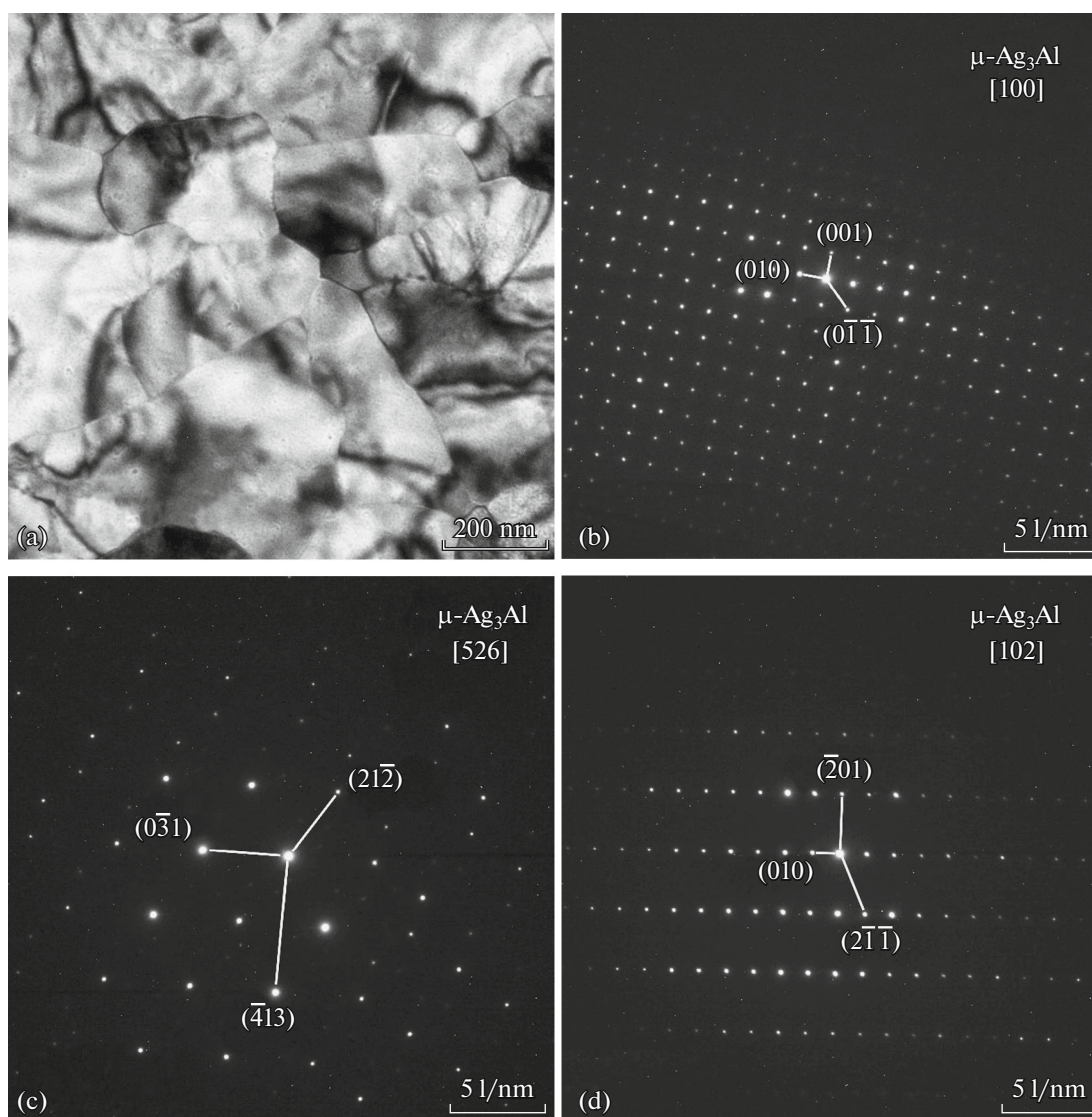


**Fig. 2.** (a) Electron microscopy image and (b, c, d) electron diffraction pattern of the Al/Ag film after heating to 300°C at different crystallite orientations.

formation during the solid-state reaction and the temperature regions of existence of these phases.

At a temperature of 107°C, weak diffraction polycrystal-type reflections corresponding to the  $\gamma$ -Ag<sub>2</sub>Al intermetallic phase were detected on the electron diffraction patterns. Upon further heating, an increase in the intensities of diffraction reflections of the  $\gamma$ -Ag<sub>2</sub>Al phase was observed. Upon reaching a temperature of 123°C, the weak-intensity point diffraction reflections corresponding to the  $\mu$ -Ag<sub>3</sub>Al intermetallic phase were detected. Upon further heating, an increase in the intensity of the  $\mu$ -Ag<sub>3</sub>Al diffraction reflections and a decrease in the intensity of the  $\gamma$ -Ag<sub>2</sub>Al reflections were observed. In the temperature range from 167 to 300°C, the electron diffraction patterns contain diffraction reflections of only the  $\mu$ -Ag<sub>3</sub>Al phase. The

electron microscopy investigations of the Al/Ag thin films after heating to 300°C showed that the films consist of crystallites with an average size of about 150–250 nm (Fig. 2a). Figures 2b, 2c, and 2d present electron diffraction patterns obtained on individual  $\mu$ -Ag<sub>3</sub>Al crystallites with the [100], [526], and [102] orientations (Figs. 2b, 2c, and 2d, respectively).

According to the EHF (effective heat of formation) theoretical model [34], the phase with the lowest effective heat of formation  $\Delta H'$  is formed first during the solid-state reaction. The  $\Delta H'$  values for the  $\gamma$ -Ag<sub>2</sub>Al and  $\mu$ -Ag<sub>3</sub>Al phases are  $-4.09$  and  $-3.12$  kJ/mol, respectively. Thus, according to the EHF model, the intermetallic  $\gamma$ -Ag<sub>2</sub>Al phase should be formed first, which is consistent with the phase sequence Al +

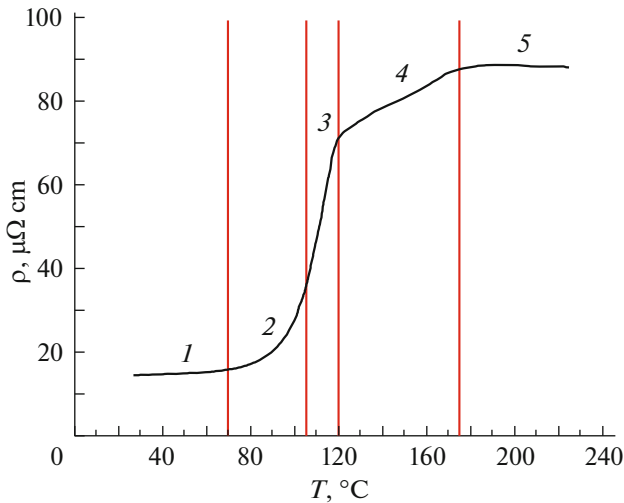


**Fig. 3.** Temperature dependence of the resistivity of the Al/Ag films during heating at an Al : Ag atomic ratio of 1 : 3.

Ag  $\xrightarrow{107^\circ\text{C}}$   $\gamma\text{-Ag}_2\text{Al}$   $\xrightarrow{123^\circ\text{C}}$   $\mu\text{-Ag}_3\text{Al}$  obtained in this work.

In order to establish the correlation between the sequence of forming phases and the electrical properties of the Al/Ag films, the resistivity variation was measured in the course of the solid-state reaction (Fig. 3). The resistivity was measured upon heating of the Al/Ag films on glass substrates in vacuum ( $1.3 \times 10^{-4}$  Pa). During the resistivity measurements, the contacts were located on the aluminum layer side.

In the initial state, the resistivity of the Al/Ag films was  $14.65 \mu\Omega \text{ cm}$ . This is similar to the value characteristic of the aluminum films with a thickness of  $\sim 20 \text{ nm}$  [35].

In the temperature range of  $25\text{--}70^\circ\text{C}$  (Fig. 3, stage 1), a slight increase in the resistivity is caused by the thermal resistivity coefficient ( $4.3 \times 10^{-3} \text{ K}^{-1}$  for silver and  $4.6 \times 10^{-3} \text{ K}^{-1}$  for aluminum [36]). In the temperature range of  $70\text{--}105^\circ\text{C}$  (Fig. 3, stage 2), the resistivity growth is close to parabolic. In this case, no changes are detected in the electron diffraction patterns. We may assume that, at this stage, the Al(Ag) and Ag(Al) solid solutions form at the interface between the aluminum and silver layers (see Fig. 4).

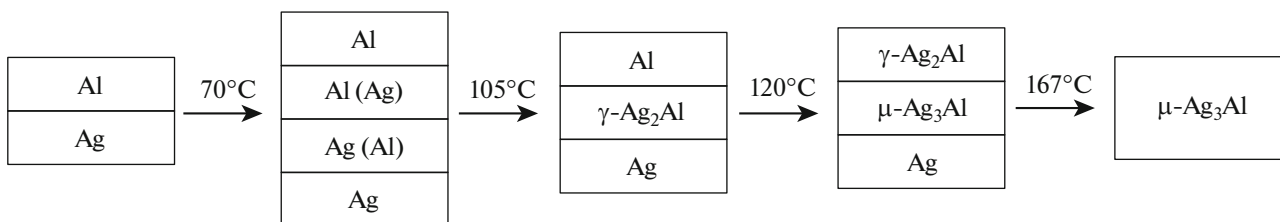


**Fig. 4.** Sequence of phases forming during the solid-state reaction in the Al/Ag films at an Al : Ag atomic ratio of 1 : 3.

The formation of the solid solutions in the Al–Ag thin films was previously observed in [24, 37]. It should be noted that, during the formation of a solid solution, the fcc aluminum layer thickness decreases, which leads to the observed increase in the resistivity.

In the temperature range of  $105\text{--}120^\circ\text{C}$  (Fig. 3, stage 3), an almost linear increase in the resistivity is observed. According to the electron diffraction data, in this temperature range, the  $\gamma\text{-Ag}_2\text{Al}$  intermetallic phase forms. It is well known that an increase in the resistance of thin films upon heating is linearly related to the thickness of intermetallic layers that form at the interface during the solid-state reaction [38]. Thus, we can assume that the change in the resistivity in the temperature range of  $105\text{--}120^\circ\text{C}$  is caused, on the one hand, by a decrease in the fcc aluminum layer and, on the other hand, by the growth of individual  $\gamma\text{-Ag}_2\text{Al}$  crystallites, which therefore form a continuous layer.

After reaching a temperature of  $\sim 120^\circ\text{C}$ , a significant decrease in the resistivity growth rate can be seen in the plot (Fig. 3, stage 4). According to the electron diffraction data, at a temperature of  $123^\circ\text{C}$ , the onset of the formation of the  $\mu\text{-Ag}_3\text{Al}$  intermetallic phase was observed. Thus, the decrease in the resistivity growth rate at  $120^\circ\text{C}$  can be explained by the fact that, upon reaching this temperature, fcc aluminum in the Al/Ag films is reacted and the  $\mu\text{-Ag}_3\text{Al}$  phase starts forming (Fig. 4). It should be noted that, in the experiments on the solid-state reaction in the Al/Ag thin films with different aluminum-to-silver atomic ratios (Al : Ag = 2 : 1, 1 : 1, and 1 : 2), only the  $\gamma\text{-Ag}_2\text{Al}$  intermetallic phase was formed [39], whereas, in this work, the formation of the  $\mu\text{-Ag}_3\text{Al}$  phase with a component ratio of Al : Ag = 1 : 3 is observed. In view of the aforesaid, one can assume that the formation of the  $\mu\text{-Ag}_3\text{Al}$  phase in the thin (up to 100 nm) films requires a significant excess of silver over aluminum in the atomic composition. In this case, the  $\mu\text{-Ag}_3\text{Al}$  phase starts forming only after fcc aluminum in the film is exhausted, which can be caused by the features of the kinetics of the solid-state reaction between aluminum and silver [40]. As was shown in [41, 42], the fast diffusion of atoms along grain boundaries during the solid-state reaction in thin films can lead to a decrease in the rate or complete suppression of the nucleation of some phases.

The growth of the  $\mu$ -Ag<sub>3</sub>Al phase is implemented at the expense of  $\gamma$ -Ag<sub>2</sub>Al and fcc silver. According to the electron diffraction data, the  $\gamma$ -Ag<sub>2</sub>Al and fcc silver phases exist in the film up to  $\sim 167^\circ\text{C}$  (Fig. 4). This is consistent with the measured resistivity data, which show that, after reaching  $\sim 175^\circ\text{C}$ , the resistivity stops growing and stabilizes at  $\sim 88 \mu\Omega \text{ cm}$  (Fig. 3, stage 5). This is related to the fact that only the  $\mu$ -Ag<sub>3</sub>Al phase remains in the film (Fig. 4).

The resistivity of the film after cooling down to room temperature was  $80.4 \mu\Omega \text{ cm}$ . The resistivity is  $\sim 30 \mu\Omega \text{ cm}$  for the  $\gamma$ -Ag<sub>2</sub>Al phase in the bulk state and  $\sim 40 \mu\Omega \text{ cm}$  for the Ag<sub>3</sub>Al phase [43]. In the Al–Ag films with a thickness of  $\sim 3 \mu\text{m}$  and crystallite size of  $\sim 1 \mu\text{m}$ , the resistivity is  $34.4 \mu\Omega \text{ cm}$  for the  $\gamma$ -Ag<sub>2</sub>Al phase and  $51.9 \mu\Omega \text{ cm}$  for the  $\mu$ -Ag<sub>3</sub>Al phase [43]. In this work, the resistivity of the  $\mu$ -Ag<sub>3</sub>Al phase ( $80.4 \mu\Omega \text{ cm}$ ) is much higher, which is explained by the significantly smaller thickness of the Al–Ag films, as well as by the relatively small crystallite size.

#### 4. CONCLUSIONS

Using in situ electron diffraction and in situ electrical resistivity measurements, the structural phase transitions occurring during the solid-state reaction in the Al/Ag thin films with an atomic ratio of Al : Ag = 1 : 3 and a total thickness of 80 nm were studied. The use of these two methods allowed us to establish the temperature of the onset of the solid-state reaction between the aluminum and silver nanolayers and propose a model of structural phase transitions during the reaction. An analysis of the resistivity measurement data allowed us to determine the temperature of the onset of the solid-state reaction and the temperature at which fcc aluminum is completely reacted. This information cannot be obtained by analyzing the electron diffraction patterns of the Al–Ag system, since the Al and Ag fcc lattice parameters differ by only 0.9%. The solid-state reaction at the interface between aluminum and silver nanolayers begins at  $70^\circ\text{C}$  with the formation of the Al–Ag solid solution, in which, upon further heating at  $105^\circ\text{C}$ , crystallites of the  $\gamma$ -Ag<sub>2</sub>Al intermetallic start forming. Upon further heating at  $120^\circ\text{C}$ , all fcc aluminum available for the reaction is reacted, which leads to the onset of the formation of the  $\mu$ -Ag<sub>3</sub>Al phase. The  $\mu$ -Ag<sub>3</sub>Al phase grows by the expense of the  $\gamma$ -Ag<sub>2</sub>Al and fcc silver phases. It was assumed that the condition for the formation of the  $\mu$ -Ag<sub>3</sub>Al phase in the course of the solid-state reaction in the Al/Ag thin (up to 100 nm) films is a significant excess of silver over aluminum in the atomic composition. It was shown that the formation of the  $\mu$ -Ag<sub>3</sub>Al phase begins only when fcc aluminum in the film is exhausted, which can be related to the kinetics of the solid-state reaction between aluminum and silver.

#### FUNDING

This study was supported by the Russian Science Foundation, project no. 18-13-00080.

#### CONFLICT OF INTEREST

The authors declare that they have no conflicts of interest.

#### REFERENCES

1. M. Schneider-Ramelow and C. Ehrhardt, *Microelectron. Reliab.* **63**, 336 (2016).
2. S. W. Fu and C. C. Lee, *J. Mater. Sci. Mater. Electron.* **29**, 3985 (2018).
3. E. Colgan, *Mater. Sci. Rep.* **5**, 1 (1990).
4. C. H. Cheng, H. L. Hsiao, S. I. Chu, Y. Y. Shieh, C. Y. Sun, and C. Peng, in *Proceedings of the 2013 IEEE 63rd Electron. Components Technology Conference, 2013*, p. 1569.
5. A. Mamala, T. Knych, P. Kwasniewski, A. Kawecki, G. Kiesiewicz, E. Sieja-Smaga, W. Sciężor, M. Gnięczyk, and R. Kowal, *Arch. Met. Mater.* **61**, 1875 (2016).
6. Y. Wang, T. L. Alford, and J. W. Mayer, *J. Appl. Phys.* **86**, 5407 (1999).
7. Y. T. Hwang, H. G. Hong, T. Y. Seong, D. S. Leem, T. Lee, K. K. Kim, and J. O. Song, *Mater. Sci. Semicond. Proc.* **10**, 14 (2007).
8. M. Qian, X. B. Shi, J. Ma, J. Liang, Y. Liu, Z. K. Wang, and L. S. Liao, *RSC Adv.* **5**, 96478 (2015).
9. J. H. Im, K. T. Kang, S. H. Lee, J. Y. Hwang, H. Kang, and K. H. Cho, *Org. Electron. Phys. Mater. Appl.* **33**, 116 (2016).
10. D. J. Kim and H. N. Lee, *Mol. Cryst. Liq. Cryst.* **645**, 185 (2017).
11. P. Afzali, M. Yousefpour, and E. Borhani, *J. Mater. Res.* **31**, 2457 (2016).
12. M. G. Blaber, M. D. Arnold, and M. J. Ford, *J. Phys.: Condens. Matter* **22**, 143201 (2010).
13. S. Auer, W. Wan, X. Huang, A. G. Ramirez, and H. Cao, *Appl. Phys. Lett.* **99**, 1 (2011).
14. K. H. Jung, S. J. Yun, S. H. Lee, Y. J. Lee, K. S. Lee, J. W. Lim, K. B. Kim, M. Kim, and R. E. I. Schropp, *Sol. Energy Mater. Sol. Cells* **145**, 368 (2016).
15. Y. J. Lee, C. B. Yeon, S. J. Yun, K. S. Lee, J. W. Lim, K. B. Kim, and J. Baek, *Mater. Res. Bull.* **48**, 5093 (2013).
16. M. K. M. Ali, K. Ibrahim, and E. M. Mkawi, *Mater. Sci. Semicond. Proc.* **16**, 593 (2013).
17. K. Meyer, *Physico-Chemical Crystallography* (VEB Deutscher Verlag Grundstoffindustrie, Leipzig, 1977).
18. D. E. Eakins, D. F. Bahr, and M. G. Norton, *J. Mater. Sci.* **39**, 165 (2004).
19. C. Xu, T. Sritharan, and S. G. Mhaisalkar, *Scr. Mater.* **56**, 549 (2007).
20. C. Weaver and D. T. Parkinson, *Philos. Mag.* **22**, 377 (1970).
21. S. Didilev, *Kompon. Tekhnol.*, No. 5, 15 (2010).
22. J. E. E. Baglin, F. M. D'Heurle, and W. N. Hammer, *J. Appl. Phys.* **50**, 266 (1979).

23. R. Roy and S. K. Sen, *J. Mater. Sci.* **27**, 6098 (1992).
24. J. Schleiweis and G. Schmitz, *Mater. Sci. Eng. A* **327**, 94 (2002).
25. A. Markwitz and W. Matz, *Interface* **26**, 160 (1998).
26. S. M. Zharkov, E. T. Moiseenko, R. R. Altunin, N. S. Nikolaeva, V. S. Zhigalov, and V. G. Myagkov, *JETP Lett.* **99**, 405 (2014).
27. E. T. Moiseenko, R. R. Altunin, and S. M. Zharkov, *Phys. Solid State* **59**, 1233 (2017).
28. S. M. Zharkov, E. T. Moiseenko, and R. R. Altunin, *J. Solid State Chem.* **269**, 36 (2019).
29. S. M. Zharkov, R. R. Altunin, E. T. Moiseenko, G. M. Zeer, S. N. Varnakov, and S. G. Ovchinnikov, *Solid State Phenom.* **215**, 144 (2014).
30. R. R. Altunin, E. T. Moiseenko, and S. M. Zharkov, *Phys. Solid State* **62**, 200 (2020).
31. E. T. Moiseenko, R. R. Altunin, and S. M. Zharkov, *Metall. Mater. Trans. A: Phys. Met. Mater. Sci.* **51**, 1428 (2020).  
<https://doi.org/10.1007/s11661-019-05602-5>
32. V. G. Myagkov, L. E. Bykova, O. A. Bayukov, V. S. Zhigalov, I. A. Tambasov, S. M. Zharkov, A. A. Matsynin, and G. N. Bondarenko, *J. Alloys Compd.* **636**, 223 (2015).
33. V. G. Myagkov, V. S. Zhigalov, L. E. Bykova, S. M. Zharkov, A. A. Matsynin, M. N. Volochaev, I. A. Tambasov, and G. N. Bondarenko, *J. Alloys Compd.* **665**, 197 (2016).
34. R. Pretorius, T. Marais, and C. Theron, *Mater. Sci. Rep.* **10**, 1 (1993).
35. J. M. Camacho and A. I. Oliva, *Thin Solid Films* **515**, 1881 (2006).
36. W. Martienssen and H. Warlimont, *Springer Handbook of Condensed Matter and Materials Data* (Springer, Berlin, 2005).
37. H. Aboulfadl, I. Gallino, R. Busch, and F. Mücklich, *J. Appl. Phys.* **120**, 195306 (2016).
38. M. Braunovic and N. Alexandrov, *IEEE Trans. Components, Packag. Manuf. Technol. A* **17**, 78 (1994).
39. R. R. Altunin, E. T. Moiseenko, N. S. Nikolaeva, and S. M. Zharkov, *Reshetn. Chten.* **1**, 590 (2016).
40. A. Gusak, F. Hodaj, and O. Liashenko, *Philos. Mag. Lett.* **95**, 110 (2015).
41. V. I. Dybkov, *J. Mater. Sci.* **22**, 4233 (1987).
42. R. W. Balluffi and J. M. Bkakey, *Thin Solid Films* **25**, 363 (1975).
43. S. Pfeifer, S. Grossmann, H. Willing, and H. Kappl, in *Proceedings of the ICEC 2014 27th International Conference on Electric Contacts, 2014*, p. 468.

*Translated by E. Bondareva*